Electrochemical Materials and Technologies

ARTICLE

Electrochemical Materials and Technologies

eISSN: 2949-0561

Cite this: Electrochem. Mater. Technol. 3 (2024) 20243032

Structure and properties of the FLiNaK – LaF_3 melt obtained with neural network potential

Dmitry Zakiryanov [a *]

Received: 21 March 2024
Accepted: 10 April 2024
Published online: 16 April 2024

DOI: 10.15826/elmattech.2024.3.032

Accurate and efficient prediction of the thermochemical properties of the melts applicable in molten salt reactors could be made if the proper machine learning model is used. In this paper, the neural network potential for simulation of 85 % $(LiF – NaF – KF)_{eut.}$ – 15 % LaF_3 molten mixture was developed based on *ab initio* data. In spite of multiple atomic types, the model of a moderate size showed small root mean squared errors in energy and forces of 0.5 meV/atom and 39 meV/Å, respectively. Then the neural network potential was employed to calculate local structure, density, self-diffusion coefficients, heat capacity, thermal conductivity, and thermal diffusivity for a range of temperatures. We found that the addition of LaF_3 to the eutectic mixture of alkali fluorides results in a reduction the melt ability to store and transfer heat. The strong effect observed here is the reduction in heat capacity by 20–30 %. The analysis of the local structure details reveals the existence of $[LaF_6]$, $[LaF_7]$ and $[LaF_8]$ groupings, with the most probable being $[LaF_7]$ and the La – F separation averaged over the ensemble of 2.35 Å.

keywords: FLiNaK, molten salt, molecular dynamics, lanthanum fluoride, fluoride melts

1. Introduction

The development of the industrial molten salt reactors meets a number of challenges [1–4]. Among the difficulties, performing experimental studies is hampered due to the toxicity and radioactivity of relevant molten salts. To address the issue, the lanthanide salts could be used to mimic actinide salts. Similarity of physicochemical properties between LaF_3 and AmF_3 was noted in [5] and LaF_3 therefore was considered as an imitator of AmF_3. Moreover, lanthanum itself can be found in spent reactor fuel [6].

The industrially crucial properties of the melts are tightly connected with their local structure. From a theoretical point of view, it is preferential to obtain both local structure patterns and physicochemical properties within the same approach in order to avoid inconsistency in methodology. Unfortunately, relatively precise *ab initio* approaches generally struggle to obtain transport properties because of high computational demands. The machine learning potentials could serve as a valuable replacement here. Once fitted to *ab initio* data, they are able to reproduce the potential energy surface (PES) with an accuracy close to the reference method. In this paper, to obtain a comprehensive insight on both local structure patterns and physicochemical properties, we apply the DeePot-SE neural network potential [7]. Details on the fitting procedure and accuracy will be discussed in the Methods section. As an object, the mixture of LaF_3 with the LiF – NaF – KF mixture of eutectic composition (also known as FLiNaK) was chosen since FLiNaK is considered as a solvent in MSR applications [8]. Therefore, the current study is aimed to investigate the thermal properties of LaF_3 as a proxy compound of AmF_3.

The structure of alkali metal halide melts containing rare-earth metal (*REM*) halides depends qualitatively on the composition. At a low concentration, individual $[RX_n]$ (R = *REM*, X = F, Cl, Br) species are predominantly observed. Once the concentration increases, these species

a: Institute of High-Temperature Electrochemistry, Ekaterinburg 620137, Russia

* Corresponding author: dmitryz.ihte@gmail.com

tend to conjugate (for example, via sharing edges) to form loose network structures [9–12]. The most relevant to our case are the studies on fluoride melts. Dracopoulos et al. [11] investigated the local structure of LnF_3 – KF (*Ln* = La, Ce, Nd, Sm, Dy, Yb) melts using Raman spectroscopy. They found that $[LnF_6]$ species are presented in the melt throughout the studied series of compositions. The same coordination number of 6 was observed in the case of NdF_3 – LiF [13]. However, this number is not a general rule: it was shown [14, 15] that the number of fluorines in the coordination shell of *REM* could depend on both *REM* and alkali metals since LaF_3 – LiF melt contain $[LnF_7]$ and $[LnF_8]$ units. In this context, the coordination number in molten mixtures containing both KF and LiF is of a high interest.

To our knowledge, the local structure of FLiNaK – LaF_3 melt has not been studied either experimentally or theoretically. The current paper presents detailed information on the structure of this mixture as well as a number of other physicochemical properties valuable for application in MSRs.

2. Neural network potential

In this paper, we apply DeePot-SE [7] neural network potential (NNP) to study FLiNaK – LaF_3 melt. DeePot-SE calculates energy and forces on the basis of the local structure data processed via the neural network. The general idea of the atom-centered machine learning potentials is as follows. The total potential energy of the whole system is decomposed as the sum of atomic contributions:

$$E = \sum_{i=1}^{N} E_i, \quad (1)$$

where E is the potential energy of an ensemble; N is the number of atoms; E_i is the contribution of i-th atom. The latter is calculated through the flexible function of many parameters (for example, an artificial neural network); the parameters (weights) should be fitted using some reference data on energy. As an input of the function, the numerical representation of the geometry of local structure (bond lengths, angles) is used which is generally of a many-body character:

$$E_i = E_i(\vec{G}) = E_i(G_1, \dots G_j), \quad (2)$$

where, the G vector is the set of numbers characterizing the particular geometry of the local structure. The 'conversion' of the geometry to some representative set of parameters is performed by either a set of analytical functions or a neural network. More details on scalable neural network potentials can be found elsewhere [16–18].

Below, in the current section, we describe the details of the reference *ab initio* calculation and the training procedure.

2.1. *Ab initio* simulations

In order to obtain the reference data to train a model, *ab initio* molecular dynamics (AIMD) simulations were performed. The FLiNaK – LaF_3 melt was presented by an ensemble of the following composition: 15 La, 130 F, 40 Li, 10 Na, 35 K. This composition approximately corresponds to the following mole fractions: 85 % FLiNaK – 15 % LaF_3. The ensemble was simulated in cubic cells with periodic boundary conditions. Born – Oppenheimer *ab initio* molecular dynamics was performed using the cp2k code [19]. Atoms were described by combinations of corresponding double-zeta basis sets (DZVP-MOLOPT-SR-GTH in cp2k notation) and Goedecker – Teter – Hutter pseudopotentials [20]. The *ab initio* method applied to calculate energy and forces was the density functional theory with the PBE functional [21]. The optimal computational parameters for simulation of FLiNaK were reported in [22]; relying on these data, the following settings were applied in the current study: 1) the dispersion correction was not used; 2) the cutoff for the plane wave energy was set to 2000 Ry; 3) the relative cutoff was 120 Ry. To maintain the desired temperature, the Nose thermostat [23] was used with a time constant of 100 fs. Three AIMD runs were performed. The first simulation run was performed under constant pressure of 1 bar and temperature of 923 K to gain the optimal density under these conditions. The equilibrium density was found to be 2.4 g/cm^3. The second run was performed under constant optimal volume and the same temperature of 923 K for 10 ps. The third run was performed under the same (constant) volume but the temperature was set to be 1600 K in order to obtain non-optimal local structure configurations and therefore to increase the reliability of the neural network potential. In other words, increasing the temperature leads to better exploration of the potential energy surface. The length of the run at 1600 K was 3 ps. To form a dataset, only constant-volume simulations were used. Given the time step of 1 fs, 13000 data frames were collected.

2.2. Training procedure

We used the DeePMD package [7] to train the NNP. 20 % of the data frames were used to form the testing dataset, while the other frames represent the training dataset. The cutoff radius for the model was chosen to be 8 Å. The network of the descriptor consisted of two layers of 16 and 32 neurons, while the fitting net was of

two layers of 32 neurons each. The total number of the neural network optimization cycles was 200000. The learning rate ranging from 10^{-2} to 10^{-8}, decaying exponentially during the training. The root mean squared errors of the final model for energy, forces, and virials are 0.5 meV/atom, 39 meV/Å, and 2.3 meV/atom, respectively (values are obtained for the testing dataset with $T = 923$ K). In Figure 1, the correlation between DFT and NNP energies and forces is presented along with the distribution of errors.

In order to additionally verify the model, we performed constant-volume molecular dynamic simulations with the fitted NNP under the same conditions as the reference *ab initio* run at 923 K. In Figure 2, the La – F and Li – F radial distribution functions obtained with neural network molecular dynamics (NNMD) and AIMD are presented. It can be seen that the AIMD and NNMD data are match well.

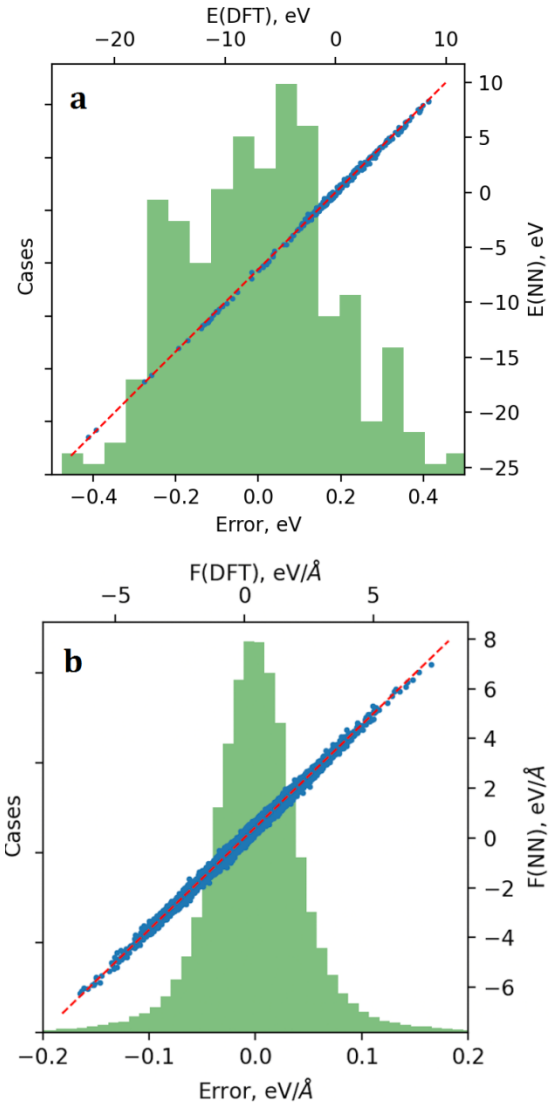

Figure 1 The correlation between the reference data and the neural network (NN) model predictions. (a: energies; b: forces. Dashed line represents the function of a perfect agreement.

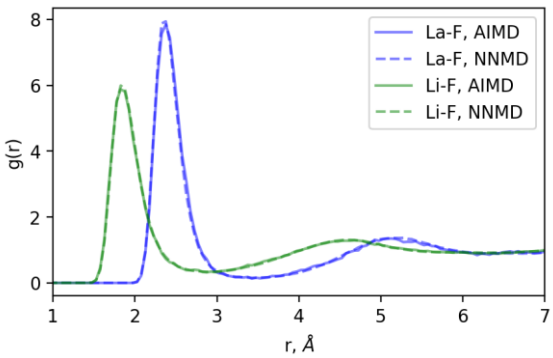

Figure 2 The radial distribution functions obtained using the reference method (AIMD, solid lines) and the trained model (NNMD, dashed lines).

Also, no unphysical behavior of the melt was observed during NNMD simulation run. A final test made here was the large-scale simulation of the ensemble of 6210 ions during 1000000 time steps under constant volume and constant temperature of 900 K. In this case we found that simulation is stable as well.

Given the results presented above, we consider the trained model to be suitable for calculating the properties.

3. Results and discussion

Using the trained NNP, properties of 85 % FLiNaK – 15 % LaF_3 molten mixture were calculated. The molecular dynamics simulations were performed using LAMMPS program [24]. Most of the properties were calculated at the temperatures of 800, 900, 1000 and 1100 K. All properties except thermal conductivity were obtained using the ensemble of 1840 ions.

3.1. Density

To evaluate the density, the ensemble was simulated under constant pressure of 1 bar with linear increase in temperature from 750 to 1100 K with a rate of 1 K/ps. The dependence of the density on temperature is presented in Figure 3. To our knowledge, no information on density of LaF_3 – FLiNaK melt was reported elsewhere. In order to deliver semi-quantitative estimation, we calculated the linear combination of FLiNaK and LaF_3 densities:

$$d_{ref} = 0.85 \cdot (2.45 - 6.53 \cdot 10^{-4} \cdot T) + \\ + 0.15 \cdot (5.793 - 6.82 \cdot 10^{-4} \cdot T). \quad (3)$$

The dependencies are taken from experimental data [25, 26] and extrapolation in the low temperature region was proposed in the case of LaF_3. Although it is a rough approximation, it can be used for comparative purposes. In Figure 3, this dependence is presented by a dashed

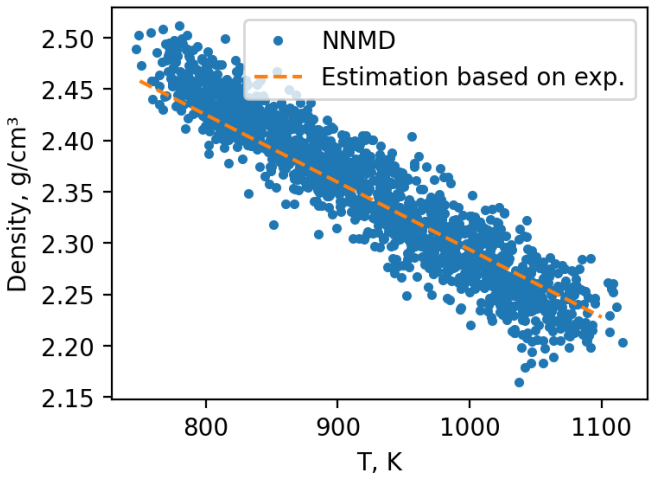

Figure 3 The density of the 85 % FLiNaK – 15 % LaF_3 melt depending on temperature. The estimation of the density based on experimental data was calculated using Equation (3).

line. It can be seen that our results agree well with Equation (3) but the slopes are somewhat different.

Linear fitting of the calculated values gives the following equation:

$$d = 3.068 - 7.78 \cdot 10^{-4} \cdot T. \quad (4)$$

3.2. Heat capacity

To estimate the heat capacity of the melt, the enthalpy of the ensemble was recorded during the run described in the previous section. Therefore, the dependence of enthalpy on temperature was obtained. Then the heat capacity at constant pressure can be calculated via:

$$C_p = \left(\frac{\partial H}{\partial T}\right)_P. \quad (5)$$

It was found that C_p is independent on temperature with the value of 1.267 J/(K · g). Note that C_p of pure FLiNaK is likely within the range of 1.769…1.883 J/(K · g) [25, 27, 28]. Therefore, the addition of 15 % LaF_3 to FLiNaK leads to a decrease in heat capacity of 20–30 %.

3.3. Local structure

Radial distribution functions (RDFs) are presented in Figure 4.

It can be seen that RDFs weakly depend on temperature with only a slight increase in peak widths at higher temperatures. The first maxima of Li – F, Na – F, and K – F RDFs are at 1.85, 2.3 and 2.6 Å, respectively, which agree well with the data on pure FLiNaK [22]. The average La – F separation is 2.35 Å while the average coordination numbers are ranging from 7.2 at 800 K to 6.9 at 1100 K. Let us analyze the La – F distribution in more detail. In Figure 5, the probabilities of certain coordination cases are plotted depending on temperature. We found that 6-, 7- and 8-fold coordinations are dominant with the contribution of other cases less than 3 %. The probability of 7-fold La is the largest, and its dependence on temperature is weak. On the other side, both 6- and 8-fold cases show significant changes with temperature: from 13 % to 33 % for the [LaF_6] and, with a reverse trend, from 30 % to 15 % for the [LaF_8]. This results in a less dense packing pattern at higher temperatures. Therefore, despite the average coordination number of La-F distribution being almost constant for the range of temperatures, the structure actually undergoes notable changes due to variable contributions of 6- and 8-fold coordinations.

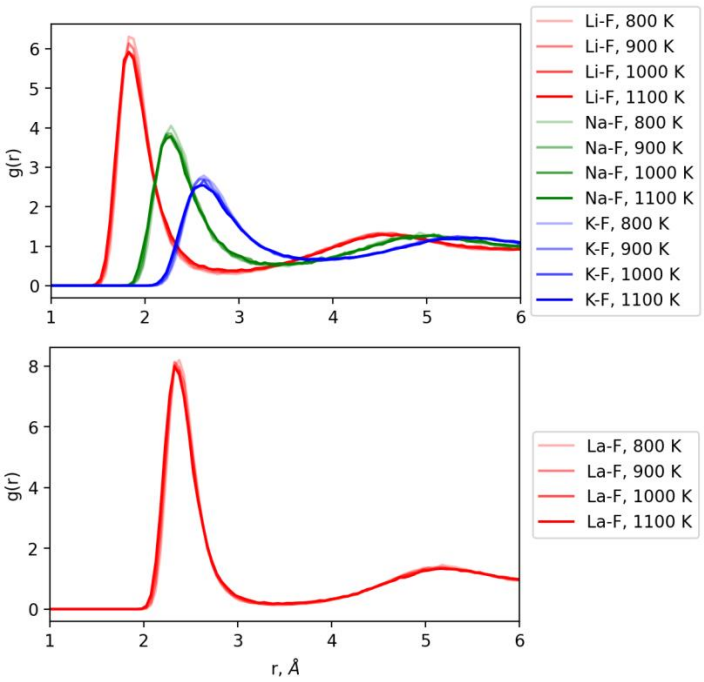

Figure 4 The radial distribution functions obtained for different temperatures.

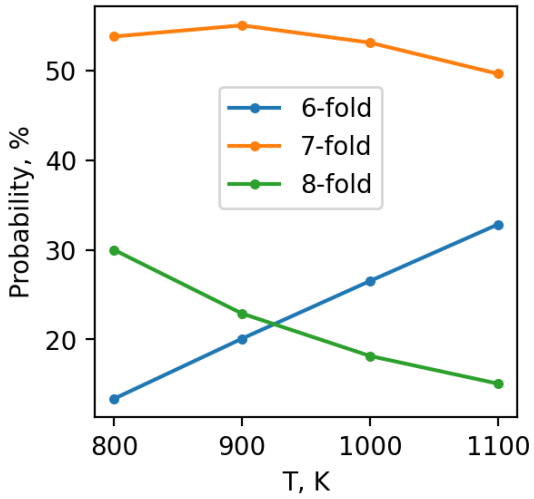

Figure 5 The probability of certain La – F coordination cases.

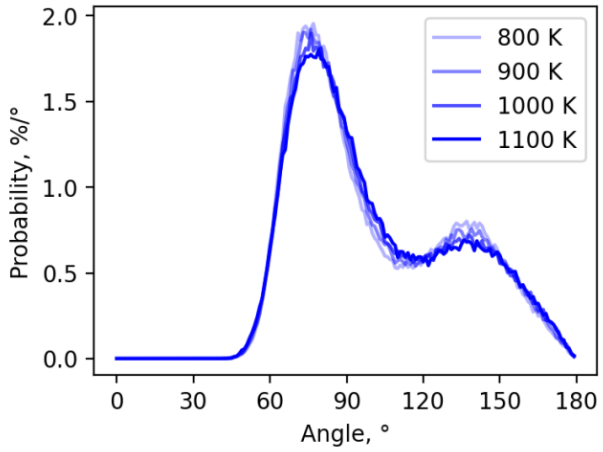

Figure 6 The F – La – F angular distribution function.

Since the [LaF_7] grouping is the most probable, the maximum of F – La – F angular distribution is less than 90 °. In Figure 6, the angular distribution function (ADF) is shown for all the temperatures studied. It can be seen that temperature has no prominent effect on ADF. The minor maximum at ~ 135 ° is produced by fluorine ions from the opposite sides of La.

3.4. Self-diffusion coefficients

Self-diffusion coefficients (SDCs) were calculated via mean squared displacements of atoms:

$$D = \lim_{\tau\to\infty}\frac{1}{6\tau}\langle|r(\tau) - r(0)|^2\rangle, \quad (6)$$

where τ is the simulation time, $r(\tau)$ is the radius vector of the atom at time τ.

The molecular dynamics was performed under constant-volume constant-temperature conditions for 500 ps at each temperature. We found that this time is enough for mean squared displacements to be well fitted by linear functions. In order to investigate the impact of the ensemble size, the simulation was performed for the large-scale ensemble of 6210 ions at 900 K. The results are presented in Figure 7a.

The size of the ensemble shows a small influence on diffusion coefficients with the largest deviation being 6 % (the case of sodium). The SDCs show strong temperature dependence. For example, the diffusion coefficient of La increases from $0.53 \cdot 10^{-9}$ to $2.51 \cdot 10^{-9}$ m²/s within the temperature range of 800 to 1100 K. At the same time, these values are the smallest among all the ions. The SDCs for Li, Na and K are close to each other while SDC of fluorine tend to be smaller. Probably, this is due to some fluorines taking part in [LaF_n] structures, and therefore the strong electrostatics hampers the transport of these fluorines through the melt. It is become more evident when taking into account

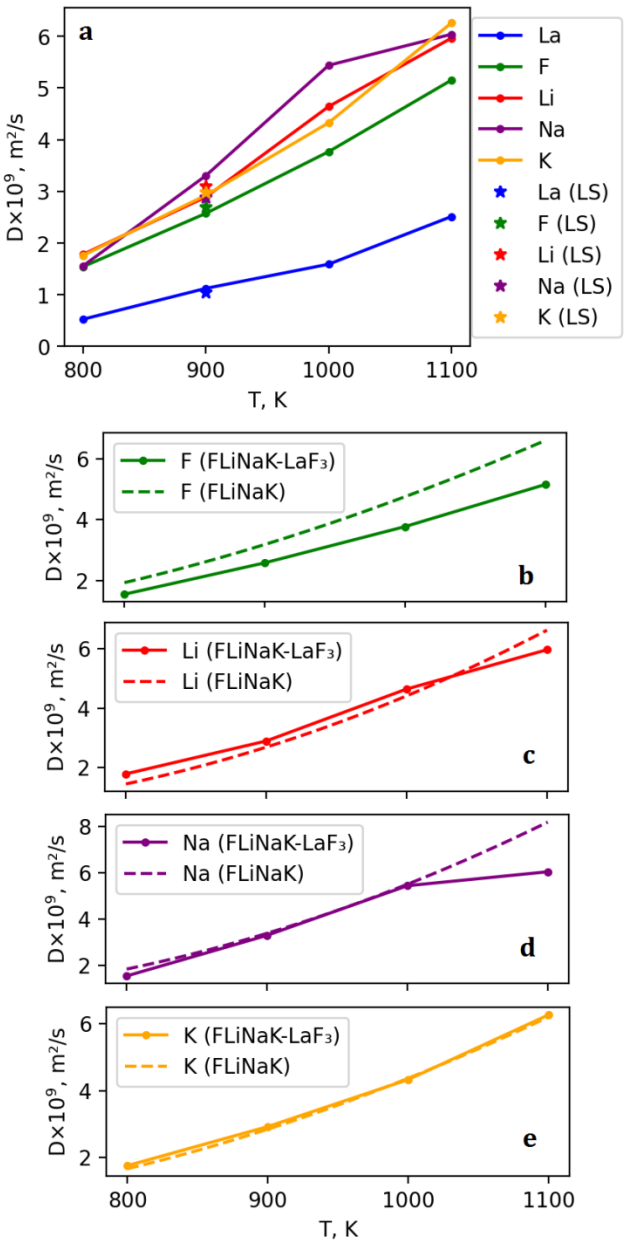

Figure 7 Self-diffusion coefficients depending on temperature. (a) – the calculated values for all atoms together; the results obtained for large-scale (LS) simulations are presented as well. (b)–(e) – the comparison of the calculated coefficients with the experimental values obtained for pure FLiNaK [29] (the extrapolation was made to cover high temperatures).

data for pure FLiNaK [29]. Figures 7b–e represent per-ion comparison of SDCs obtained for the melt with and without LaF_3. It can be seen that self-diffusion coefficients of all ions are generally match, except the case of fluorine. In FLiNaK – LaF_3 melt, the SDC for fluorine is lower by 25 – 29 %. Such close values for pure and LaF_3-containing melt are a bit disturbing since the latter is expected to have lower rate of mass transport. Chesser, Gou and Zhang studied [30] La diffusion in FLiNaK with the LaF_3 content lower by an order of magnitude compared to our study. For 1000 K, the value of the lanthanum SDC calculated using the equation proposed

by them is $D_{La} = 0.33 \cdot 10^{-9}$ m²/s. For comparison, NNP predicts $D_{La} = 1.59 \cdot 10^{-9}$ m²/s at 1000 K. This forces us to assume that the values of diffusion coefficients obtained with NNP are likely overestimated; to some extent, this could be explained by lacking dispersion interactions which were excluded in reference *ab initio* calculations due to observations reported in [22].

3.5. Thermal conductivity and thermal diffusivity

The issue of thermal conductivity remains open even in the case of pure FLiNaK. The values of the thermal conductivity coefficient λ obtained in different studies vary in both quantitative and qualitative terms.

While some sources report an increase in λ with temperature [30, 31, 32], others show either the opposite or unclear temperature dependence [33, 34]. In most cases, the values lie within the range of 0.75…0.85 W/(m · K).

To calculate the thermal conductivity coefficient of 85 % FLiNaK – 15 % LaF_3 melt, the non-equilibrium approach was used. The elongated molecular dynamic cell contained 2300 ions. The heating and cooling layers were defined in the cell as shown in Figure 8a. The heating/cooling rate was set to be ± 0.2 eV/ps. As a consequence of the finite speed of heat exchange, the temperature gradient appears in the cell. Then the thermal conductivity coefficient λ can be estimated via the following formula:

$$\lambda = -\frac{Q}{\Delta T} \cdot \frac{l_z}{2}, \quad (7)$$

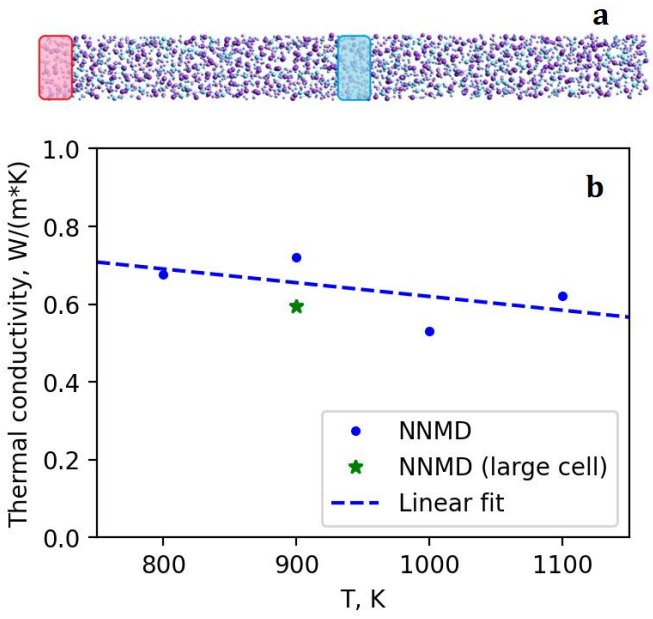

Figure 8 a: The molecular dynamic cell for calculating thermal conductivity coefficient. The heating and cooling layers are highlighted in red and blue. b: The calculated thermal conductivity coefficient depending on temperature.

where Q is the heat flux, ΔT is the temperature difference between the heating and cooling layers, l_z is the cell length along the direction of the temperature gradient.

The simulations were performed for 1 ns with the averaging performed over last 0.9 ns. The ensemble was simulated under constant energy conditions. In order to ensure energy conservation, the time step of 0.25 fs was used. The calculated thermal conductivity coefficients are presented in Figure 8b. For the studied temperature range, the values of λ range from 0.53 to 0.72 W/(m · K). The linear fit shows negative temperature dependence:

$$\lambda = 0.9738 - 3.54 \cdot 10^{-4} \cdot T. \quad (8)$$

Apparently, the addition of 15 % LaF_3 lead to slight reduce in thermal conductivity although strong statement here cannot be posed due to uncertainty in data on pure FLiNaK. Additionally, the simulation of the ensemble of 4600 ions was performed at 900 K in order to test the impact of cell size. The deviation of the λ value obtained for the large ensemble is of the order of general deviations caused by finite run length.

Using the obtained density, heat capacity, and thermal conductivity, the temperature dependence of thermal diffusivity can be written as:

$$\alpha = (2.6 - 4.67 \cdot 10^{-4} \cdot T) \cdot 10^{-7}. \quad (9)$$

Therefore, the thermal diffusivity of 85 % FLiNaK – 15 % LaF_3 melt decreases from $2.23 \cdot 10^{-7}$ m²/s (T = 800 K) to $2.09 \cdot 10^{-7}$ m²/s (T = 1100 K).

4. Conclusions

Let us summarize the results of the simulations. Our neural network interatomic potential (NNP) relies on *ab initio* data obtained using DFT / PBE approach. Given small root mean squared errors shown by NNP, it is fair to characterize the calculated properties as *ab initio*-accurate. Despite a strong lack of reference data, an indirect comparison could be made. For density, we used the additive estimation while for other properties we compared with pure FLiNaK. It was found that the addition of 15 % LaF_3 to FLiNaK results in reduction of heat capacity and thermal conductivity. Both of these are undesirable effects for MSR applications since the ability of the salt to store and transfer thermal energy would be smaller.

Another point addressed in this study was the local structure. It was noted that La coordination in fluoride melts depends on salt composition: [LnF_6] is typical for

LnF_3 – KF [13], while LaF_3 – LiF contains $[LaF_7]$ and $[LaF_8]$ [14, 15]. FLiNaK represents here an intermediate case and it fits well with previous observations that we found $[LaF_6]$, $[LaF_7]$ and $[LaF_8]$ to exist in the FLiNaK – LaF_3 molten mixture. About half of the cases are represented by $[LaF_7]$, while the contributions of $[LaF_6]$ and $[LaF_8]$ depend on temperature: at higher temperatures, the less dense $[LaF_6]$ grouping is preferential.

Final comment should be given here is one on the dispersion correction. In this study, reference simulations lacking such a correction. On the one hand, the calculated density values are reasonable, although the verification rely on rough approximation due to absence of other reference data. On the other hand, the obtained diffusion coefficients were apparently overestimated. It can be suggested that inclusion / exclusion of the dispersion correction leads to property-dependent changes in accuracy; further investigations for fluoride melts should be made here to find the balanced computational approach.

Supplementary materials

No supplementary materials are available.

Funding

This research had no external funding.

Acknowledgments

None.

Author contributions

Dmitry Zakiryanov: Conceptualization; Data curation; Formal Analysis; Writing – Original draft.

Conflict of interest

The authors declare no conflict of interest.

Additional information

Dmitry Zakiryanov, Author ID: 57190936802; Orcid: 0000-0003-2649-7871.

References

1. Ignatiev VV, Feynberg OS, Zagnitko AV, Merzlyakov AV, et al., Molten-salt reactors: new possibilities, problems and solutions, Atomic Energy, **112** (2012) 157–165. https://doi.org/10.1007/s10512-012-9537-2

2. LeBlanc D, Molten salt reactors: A new beginning for an old idea, Nuclear Engineering and Design, **240(6)** (2010) 1644–1656. https://doi.org/10.1016/j.nucengdes.2009.12.033

3. Serp J, Allibert M, Beneš O, Delpech S, et al., The molten salt reactor (MSR) in generation IV: Overview and perspectives, Progress in Nuclear Energy, **77** (2014) 308–319. https://doi.org/10.1016/j.pnucene.2014.02.014

4. Roper R, Harkema M, Sabharwall P, Riddle C, et al., Molten salt for advanced energy applications: A review, Annals of Nuclear Energy, **169** (2022) 108924. https://doi.org/10.1016/j.anucene.2021.108924

5. Ponomarev LI, Seregin MB, Mihalichenko AA, Parshin AP, et al., Substantiation of the choice of actinide fluoride imitators for the study of solubility in the fuel salt of molten-salt reactors (in Russian), Atom. Energiya, **112** (2012).

6. Ackerman JP, Chemical basis for pyrochemical reprocessing of nuclear fuel, Industrial & Engineering Chemistry Research., **30(1)** (1991) 141–145. https://doi.org/10.1021/ie00049a022

7. Wang H, Zhang L, Han J, E W, DeePMD-kit: A deep learning package for many-body potential energy representation and molecular dynamics, Computer Physics Communications, **228** (2018) 178–84. https://doi.org/10.1016/j.cpc.2018.03.016

8. Bahri CNACZ, Al-Areqi WM, MIRuf FM, Majid AA, Characteristic of molten fluoride salt system LiF-BeF_2 (Flibe) and LiF-NaF-KF (Flinak) as coolant and fuel carrier in molten salt reactor (MSR), AIP Conference Proceedings, **1799** (2017) 040008. https://doi.org/10.1063/1.4972932

9. Dracopoulos V, Gilbert B, Brrensen B, Photiadis GM, et al., Vibrational modes and structure of rare earth halide–alkali halide binary melts YBr_3–ABr (A=Li, K, Cs) and YF_3–KF, Journal of the Chemical Society, Faraday Transactions, **93** (1997) 3081–3088. https://doi.org/10.1039/a701864i

10. Photiadis GM, Brresen B, Papatheodorou GN, Vibrational modes and structures of lanthanide halide–alkali halide binary melts $LnBr_3$–KBr (Ln=La, Nd, Gd) and $NdCl_3$–ACl (A=Li, Na, K, Cs), Journal of the Chemical Society, Faraday Transactions, **94** (1998) 2605–2613. https://doi.org/10.1039/a802813c

11. Dracopoulos V, Gilbert B, Papatheodorou GN, Vibrational modes and structure of lanthanide fluoride–potassium fluoride binary melts LnF_3–KF (Ln=La, Ce, Nd, Sm, Dy, Yb), Journal of the Chemical Society, Faraday Transactions, **94** (1998) 2601–2604. https://doi.org/10.1039/a802812e

12. Fukushima K, Yamoto H, Iwadate Y, Raman spectroscopic study of molten $SmCl_3$–ACl systems (A=Li, Na, K), Journal of Alloys and Compounds, **290(1–2)** (1999) 114–118. https://doi.org/10.1016/s0925-8388(99)00216-9

13. Stefanidaki E, Photiadis GM, Kontoyannis CG, Vik AF, et al., Oxide solubility and Raman spectra of NdF_3–LiF–KF–MgF_2–Nd_2O_3 melts, Journal of the Chemical Society, Dalton Transactions, (2002) 2302–2307. https://doi.org/10.1039/b111563b

14. Rollet A-L, Godier S, Bessada C, High temperature NMR study of the local structure of molten LaF_3–AF (A = Li, Na, K and Rb) mixtures, Physical Chemistry Chemical Physics, **10** (2008) 3222–3228. https://doi.org/10.1039/b719158h

15. Bessada C, Rakhmatullin A, Rollet A-L, Zanghi D, High temperature NMR approach of mixtures of rare earth and alkali fluorides: An insight into the local structure, Journal of Fluorine Chemistry, **130(1)** (2009) 45–52. https://doi.org/10.1016/j.jfluchem.2008.07.010

16. Deringer VL, Caro MA, Csányi G, Machine Learning Interatomic Potentials as Emerging Tools for Materials Science, Advanced Materials, **31(46)** (2019) 1902765. https://doi.org/10.1002/adma.201902765

17. Mortazavi B, Zhuang X, Rabczuk T, Shapeev AV, Atomistic modeling of the mechanical properties: the rise of machine learning interatomic potentials, Materials Horizons, **10** (2023) 1956–1968. https://doi.org/10.1039/d3mh00125c

18. Mueller T, Hernandez A, Wang C, Machine learning for interatomic potential models, The Journal of Chemical Physics, **152(5)** (2020) 050902. https://doi.org/10.1063/1.5126336

19. Hutter J, Iannuzzi M, Schiffmann F, VandeVondele J, Cp2k: atomistic simulations of condensed matter systems, Wiley Interdiscip, Rev.: Comput. Mol. Sci., **4(1)** (2014) 15–25, https://doi.org/10.1002/wcms.1159

20. VandeVondele J, Hutter J, Gaussian basis sets for accurate calculations on molecular systems in gas and condensed phases, J Chem. Phys., **127(11)** (2007) 114105. https://doi.org/10.1063/1.2770708

21. Perdew JP, Burke K, Ernzerhof M, Generalized Gradient Approximation Made Simple, Phys. Rev. Lett., **77** (1996) 3865–3868. https://doi.org/10.1103/physrevlett.77.3865

22. Frandsen BA, Nickerson SD, Clark AD, Solano A, et al., The structure of molten FLiNaK, Journal of Nuclear Materials, **537** (2020) 152219. https://doi.org/10.1016/j.jnucmat.2020.152219

23. Nosé S, A unified formulation of the constant temperature molecular dynamics methods, J Chem. Phys., **81** (1984) 511–519. https://doi.org/10.1063/1.447334

24. Thompson AP, Aktulga HM, Berger R, Bolintineanu DS, et al., LAMMPS - a flexible simulation tool for particle-based materials modeling at the atomic, meso, and continuum scales, Computer Physics Communications, **271** (2022) 108171. https://doi.org/10.1016/j.cpc.2021.108171

25. An X-H, Cheng J-H, Su T, Zhang P, Determination of thermal physical properties of alkali fluoride/carbonate eutectic molten salt, AIP Conference Proceedings, **1850(1)** (2017) 070001. https://doi.org/10.1063/1.4984415

26. Janz GJ. Thermodynamic and Transport Properties for Molten Salts: Correlation Equations for Critically Evaluated Density Surface Tension Electrical Conductance and Viscosity Data. Part 17. New York: American Chemical Society and the American Institute of Physics; 1988. 309 p.

27. Salanne M, Simon C, Turq P, Madden PA, Heat-transport properties of molten fluorides: Determination from first-principles, J. Fluor. Chem., **130(1)** (2009) 38–44, https://doi.org/10.1016/j.jfluchem.2008.07.013

28. Ingersoll DT, Forsberg CW, MacDonald PE. Trade Studies for the Liquid-Salt-Cooled Very High-Temperature Reactor: Fiscal Year 2006 Progress Report. Oak Ridge National Laboratory, Oak Ridge, Tennessee; 2007. 265 p.

29. Umesaki N, Iwamoto N, Tsunawaki Y, Ohno H, Furukawa K, Self-diffusion of lithium, sodium, potassium and fluorine in a molten LiF + NaF + KF eutectic mixture, Journal of the Chemical Society, Faraday Transactions 1: Physical Chemistry in Condensed Phases, **77** (1981) 169–175. https://doi.org/10.1039/f19817700169

30. Chesser R, Guo S, Zhang J, Electrochemical behavior of dysprosium and lanthanum in molten LiF-NaF-KF (Flinak) salt, Annals of Nuclear Energy, **120** (2018) 246–252. https://doi.org/10.1016/j.anucene.2018.05.045

31. Robertson SG, Wiser R, Yang W, Kang D, et al., The curious temperature dependence of fluoride molten salt thermal conductivity, Journal of Applied Physics, **131(22)** (2022) 225102. https://doi.org/10.1063/5.0088059

32. Smirnov M, Khokhlov V, Filatov E, Thermal conductivity of molten alkali halides and their mixtures, Electrochimica Acta, **32(7)** (1987) 1019–1026. https://doi.org/10.1016/0013-4686(87)90027-2

33. Gallagher RC, Birri A, Russell NG, Phan A-T, et al., Investigation of the thermal conductivity of molten LiF-NaF-KF with experiments, theory, and equilibrium molecular dynamics, Journal of Molecular Liquids, **361** (2022) 119151. https://doi.org/10.1016/j.molliq.2022.119151

34. Rudenko A, Redkin A, Il'ina E, Pershina S, et al., Thermal Conductivity of FLiNaK in a Molten State, Materials, **15(16)** (2022) 5603. https://doi.org/10.3390/ma15165603